The Asteroseismic Imprints of Mass Transfer

TOM WAGG [ID],[1, 2] COLE JOHNSTON [ID],[3, 4] EARL P. BELLINGER [ID],[2, 5] MATHIEU RENZO [ID],[6] AND SELMA E. DE MINK [ID][2]

[1]*Department of Astronomy, University of Washington, Seattle, WA, 98195*
[2]*Max-Planck-Institut für Astrophysik, Karl-Schwarzschild-Straße 1, 85741 Garching, Germany*
[3]*Department of Astrophysics, IMAPP, Radboud University Nijmegen, PO Box 9010, 6500 GL Nijmegen, The Netherlands*
[4]*Institute of Astronomy, KU Leuven, Celestijnenlaan 200D, 3001 Leuven, Belgium*
[5]*Department of Astronomy, Yale University, CT, 06511, USA*
[6]*Center for Computational Astrophysics, Flatiron Institute, 162 Fifth Ave, New York, NY, 10010, USA*

ABSTRACT

We present new simulations investigating the impact of mass transfer on the asteroseismic signals of slowly pulsating B stars. We use `MESA` to simulate the evolution of a binary star system and `gyre` to compute the asteroseismic properties of the accretor star. We show that, compared to a single star of the same final mass, a star that has undergone accretion has a significantly different internal structure, evident in both the hydrogen abundance profile and Brunt–Väisälä frequency profile. These differences result in significant changes in the observed period spacing patterns, implying that one may use this as a diagnostic to test whether a star's core has been rejuvenated as a result of accretion. We show that one may draw misleading conclusions of stellar properties when only assuming single star evolution in fitting procedures. Our proof of principle analysis demonstrates the need to further investigate the impact of binary interactions on stellar asteroseismic signals for a wide range of parameters, such as initial mass, amount of mass transferred and the age of the accretor star at the onset of mass transfer.

Corresponding author: Tom Wagg
tomjwagg@gmail.com

1. INTRODUCTION

The majority of massive stars are born in binaries and multiple systems (e.g. Mason et al. 2009; Almeida et al. 2017; Moe & Di Stefano 2017), a large subset of which will exchange mass (e.g Sana et al. 2012). However, mass transfer, both the process itself and the impact it has on the component stars, is still highly uncertain. This means that there are large uncertainties in evolutionary calculations and predictions, such as the rate of formation of close double compact objects and gravitational wave sources (e.g. Broekgaarden et al. 2022).

There are still many uncertainties in the effect that mass transfer has on mass-gainers, despite the many investigations into understanding the diversity of mass-losers.

Cole: Could you point me to some of these or a starting paper I can use to find the rest?

Among these uncertainties a key question is whether a mass-gainer will be rejuventated, where convective cores in accretors grow to account for the additional mass (e.g. Neo et al. 1977), and if so, to what extent. To date, there is no strong observational diagnostic for determining whether the core of a star has been rejuvenated.

Asteroseismology probes the internal structure of stars and so may hold the key to constraining rejuvenation. It is well established that asteroseismology can be used to estimate precise stellar masses, radii and ages based on stellar oscillation modes (Aerts et al. 2010). In particular, main sequence gravity (g) mode pulsators can be observed deep into their radiative envelopes using high-order g-mode oscillations. These pulsators include Slowly Pulsating B (SPB) stars, driven by the κ-mechanism (Waelkens & Rufener 1985; Waelkens 1991; Cox et al. 1992; Pamyatnykh 1999). g-mode pulsators have been used to provide insights into many aspects of stellar evolution, such as the mass of stellar cores (Johnston 2021; Pedersen 2022) internal mixing processes, and angular momentum transport (Aerts et al. 2019). Recently, g-mode asteroseismology has been used to probe the chemical and temperature gradients outisde of the cores of massive stars (Michielsen et al. 2021; Pedersen et al. 2018).

These insights into stellar properties are possible due to the intricate dependence of period spectrum of g-mode pulsations on the size of the convective core and the chemical composition gradient outside of the core (e.g. Miglio et al. 2008). Based on these measured properties, one can infer precise estimates of stellar masses and radii, as well as stellar ages and internal structure properties with additional assumptions of stellar evolution.

Current works only consider single star evolution when inferring stellar properties. However, mass transfer can profoundly influence the structure and composition gradients of accreting stars even after thermal re-adjustment, as indicated by numerous studies using 1D stellar evolution codes (Renzo & Götberg 2021; Miszuda et al. 2021). These changes in structure are usually a result of rejuvenation.

As the frequencies of self-excited stellar pulsations are finely tuned by the internal structure of stars, asteroseismology holds the potential to identify the signature of previous mass transfer in various classes of pulsating stars. Furthermore, assuming single star evolution for a star that has undergone accretion may result in misleading inferences of its stellar properties from asteroseismology.

In this paper we assess the impact that mass transfer leaves on the asteroseismic signal of pulsating stars that have recently gained mass through binary interaction. In particular we focus on SPB stars as they are numerous, easily observationally identifiable and have a relatively high binary fraction. We use the 1D stellar evolution code `MESA` to demonstrate the difference in evolution between an accreting star and an equivalent single star. Using the `GYRE` stellar oscillation code we show how these differences in evolution influence the period spacing pattern of an accreting star and highlight how this could affect the inferred properties of the star if single stellar evolution was assumed.

2. BINARY STELLAR EVOLUTION

In this Section we outline the setup of our `MESA` binary models and describe the evolution of the system, both across the Hertzsprung-Russell diagram and in terms its internal structure.

2.1. *Model setup*

We use Modules for Experiments in Stellar Astrophysics (`MESA`, Paxton et al. 2011, 2013, 2015, 2018, 2019; Jermyn et al. 2023) version r23.05.01 (Paxton 2023) to simulate non-rotating models for a binary system, as well as a grid of single stars against which to compare. Our full inlists are available on GitHub[1] and our model outputs are available on Zenodo[2].

Tom: add Zenodo links when done

In particular, the most pertinent settings that we change from the defaults for this work are as follows: We adopt the Ledoux (1947) criterion to account for

---

[1] https://github.com/TomWagg/mass-gainer-seismology
[2] https://zenodo.org/record/

the presence of a chemical gradient when determining the stability of convection. We include semiconvection following Langer et al. (1983) with a scaled efficiency of $\alpha_{\rm thm} = 0.1$. For accretors we include thermohaline mixing once they finish accretion following Kippenhahn et al. (1980) with an efficiency of $\alpha_{\rm SC} = 1$. We use exponential core overshooting from Herwig (2000), setting $(f, f_0) = (0.01, 0.005)$ (Claret & Torres 2017). We set a minimum diffusive mixing coefficient of 20 cm^2 s^{-1}; this smooths out any numerical discontinuities in the composition gradients and accounts for a lack of rotational mixing in our models. We motivate our choice of 20 cm^2 s^{-1} and highlight the effect of changing the mixing coefficient on our results in Appendix A. We follow the Kolb & Ritter (1990) prescription to the mass transfer rate with an implicit scheme. We do not account for any rotation in our models. Although we expect that a typical pulsator will likely have some level of rotation, we restrict our proof of principle analysis to less complex non-rotating models. We discuss this choice further in Section 4.3.

Our binary model has a donor with an initial mass of 4 M$_\odot$ and an accretor with an initial mass of 3 M$_\odot$, following the typical mass range of SPB stars (Waelkens & Rufener 1985; Waelkens 1991; Kurtz 2022), with an initial period of 5 days and metallicity $Z = 0.02$. We evolve this system up to Roche Lobe overflow and proceed with mass transfer until the secondary accretes 0.5 M$_\odot$. At this point we end mass transfer, detach the binary and reduce the donor to a point mass, since we are no longer interested in the properties of the donor and thus only track the evolution of the accretor from this point onwards. Although our choice of 0.5 M$_\odot$ is somewhat arbitrary, this amount could be obtained through different choices of mass transfer efficiencies and the spin-up of the accretor would likely hinder accretion in a similar manner. By constructing our model in this way we are able to account for a realistic, variable accretion rate.

> **Selma:** Help justify the binary model setup.

We then evolve the rejuvenated accretor until central hydrogen depletion. Additionally, for comparison, we evolve a grid of single stars with masses from 3-6 M$_\odot$ until the end of helium core burning.

2.2. Hertzsprung-Russell diagram evolution

In Figure 1 we show the evolution across the Hertzsprung-Russell diagram of both the donor and accretor of our binary model, with a subset of our single stellar models in the background.

The evolution of the donor (starting at D1) initially follows the 4 M$_\odot$ single star track, expanding across the main sequence, turning-off and moving across the
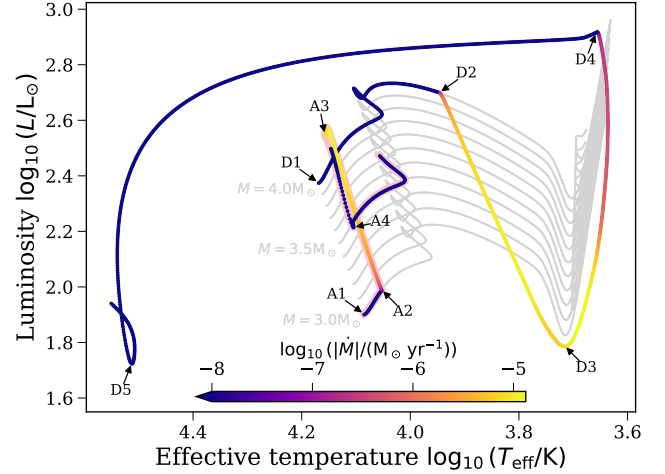
Figure 1. Hertzsprung-Russell diagram showing the evolution of the binary. Tracks are shown for both the donor and accretor, coloured by the absolute mass transfer rate. We highlight the accretor track with a pink outline. Single star tracks added as background grey curves, with masses from 3 to 4 M$_\odot$ in 0.1 M$_\odot$ intervals. Important points in the evolution are annotated with arrows and described in the text.

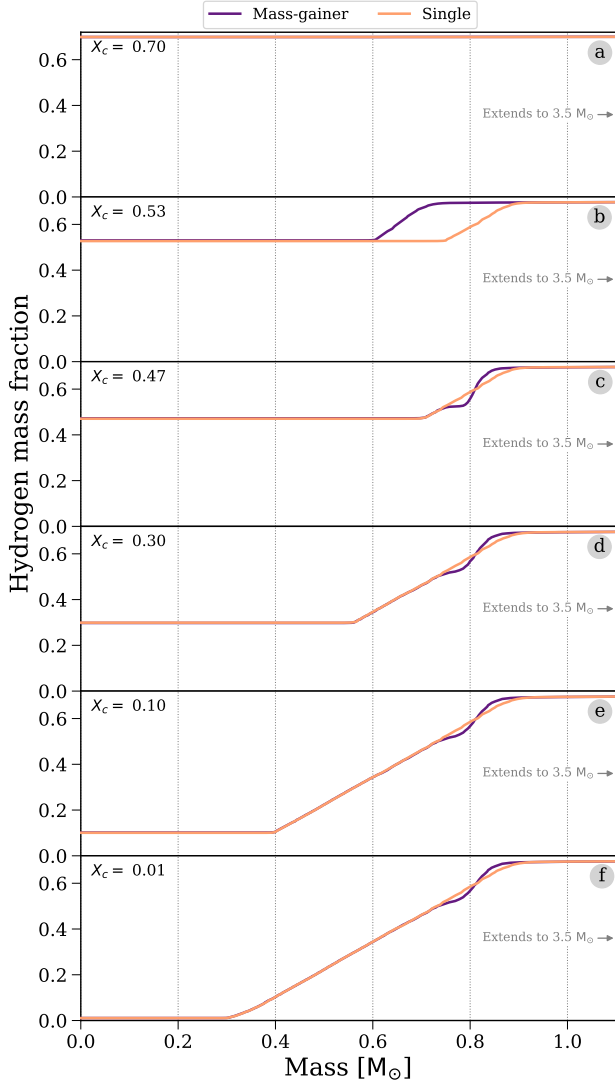> **Mathieu:** Mathieu and Selma disagree on HRD

> **Selma:** Mathieu and Selma disagree on HRD

Hertzsprung gap. Midway through the expansion on the Hertzsprung gap, at point D2, the donor overflows its Roche Lobe and diverges from the single star track, decreasing in luminosity as it transfers mass. As the mass transfer proceeds the orbit of the binary shrinks, increasing the mass transfer rate until the point of closest approach at D3. With the reversal of the mass ratio, mass transfer then causes the orbit the widen, decreasing the mass transfer rate and allowing the donor to increase in luminosity once more. Once the orbit widens to such an extent that Roche lobe overflow ceases (at point D4), the donor relaxes on a thermal timescale, before proceeding with helium core burning from point D5 onwards.

The evolution of the accretor (highlighted in pink) follows the 3 M$_\odot$ single star track initially (starting from point A1), but early into its main sequence evolution the donor initiates mass transfer (at point A2) and the accretor increases in luminosity to compensate. Once mass transfer ceases at point A3, the accretor returns to thermal equilibrium at point A4 and proceeds with its main sequence evolution along the 3.5 M$_\odot$ single star track.
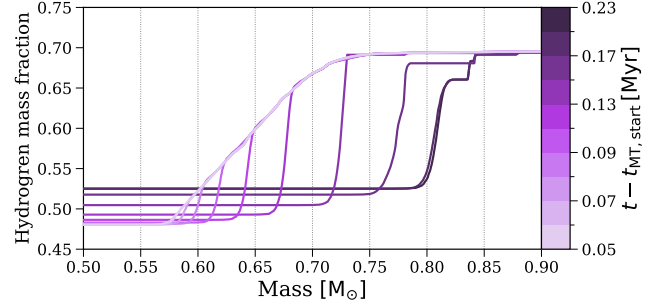
2.3. Rejuvenation and chemical gradients

Although the accretor appears to simply follow a more massive single star track in the Hertzsprung-Russell di-

Figure 2. Comparison of the hydrogen abundance profiles between (i) an initially $3\,\mathrm{M_\odot}$ star that accretes mass from a companion and (ii) a single star with the same final mass of $3.5\,\mathrm{M_\odot}$. Each panel compares the stars at the same central hydrogen abundance, which is annotated in each panel.

Figure 3. Hydrogen abundance profile of our accretor model during mass transfer. Each line is coloured by its time after the start of mass transfer. This plot shows more time-resolved evolution between panels b and c of Figure 2.

allowing radiation to travel more freely, leading to a recession of the convective core (Mitalas 1972; Crowe & Matalas 1982; Miglio et al. 2008; Silva Aguirre et al. 2011). As the core recedes it has a decreasing hydrogen abundance, and therefore it imprints a composition gradient in its wake in the abundance profile. We see these trends in Figure 2 as the single star (shown in orange) evolves, with the central abundance decreasing and the imprinted chemical composition gradient extending over time (in the region with diagonal lines).

For the mass-gainer the evolution initially proceeds in a similar manner. In panel b, the shape is similar to that of the single star, though with a smaller convective core due to the star's initially lower mass. Between panels b and c, mass transfer occurs. As mass transfer proceeds the accretor increases in luminosity to compensate for the additional mass. This leads to an increase in the convective core size, which one can see as the profiles move outwards in mass coordinates in Figure 3. At the same time this core expansion leads to a rejuvenation of the accretor as more hydrogen is mixed into the core, increasing the central abundance (Neo et al. 1977). The expansion of the core into the region through which it previously receded sharpens the composition gradient, resulting in the 'kink' in the abundance profile relative to the single star for the remaining panels of Figure 2. The origin of this feature is shown in Figure 3, where we see the hydrogen abundance increase and extend outwards as the core rejuvenates, thus washing away the previous gradient. Returning to Figure 2, the evolution of the abundance profile after mass transfer proceeds similarly to the single star, with subsequent recession of the core and a resulting composition gradient. Critically however, the feature arising from mass transfer remains throughout the main sequence (albeit marginally smoothed by internal mixing).

3. ASTEROSEISMIC SIGNALS

agram, its *internal* structure has been altered to support the incoming mass, leading to a rejuvenated core (). This is evident in the hydrogen abundance profile of the star, which we plot in Figure 2. In each panel we compare the accretor of our binary model with a $3.5\,\mathrm{M_\odot}$ single star, thus the stars have the same final mass. We highlight that in this figure mass transfer occurs between panels b and c and discuss the difference below.

First, we consider the evolution of the abundance profile for the single star. As the star evolves, it burns hydrogen in its core, decreasing the central hydrogen abundance. At the same time, the reduced hydrogen abundance decreases the opacity of the edge of the core,

In this Section we demonstrate how the differences in internal structure between the accretor and single star lead to altered asteroseismic signals. We first consider how the Brunt–Väisälä frequency profile is changed, before showing how this influences the period spacing patterns.

3.1. *Brunt–Väisälä frequency profile*

The Brunt–Väisälä frequency (Väisälä 1925; Brunt 1927), N, defines the regions in which convective instabilities can occur, such that $N^2 < 0$ indicates a convective region, and $N^2 > 0$ a radiative region in which g-modes can propagate[3]. The Brunt–Väisälä frequency directly determines the period distribution of g-mode oscillations and thus it is pertinent to consider the impact of mass transfer on it. For an ideal gas the frequency can be approximated as

$$N^2 \cong \frac{g^2 \rho}{P}(\boldsymbol{\nabla}_{\mathrm{ad}} - \boldsymbol{\nabla} + \boldsymbol{\nabla}_{\mu}), \qquad (1)$$

where ρ is the density, P is the pressure, $\boldsymbol{\nabla}_{\mathrm{ad}} = 2/5$ is the adiabatc temperature gradient and assumed to be a constant, $\boldsymbol{\nabla}$ is the temperature gradient and $\boldsymbol{\nabla}_{\mu}$ is the chemical composition gradient. We highlight that although many of the terms in this expression are similar for our accretor model and equivalent single star model, the density profile and, as noted in Section 2.3, the composition gradient $\boldsymbol{\nabla}_{\mu}$ show significant differences and as such we expect similar differences in the Brunt–Väisälä frequency profile.

In Figure 4 we compare, for the same central hydrogen content, the Brunt–Väisälä frequency profiles for the accretor star model and single star model with the same final mass. Each panel is for the same central hydrogen content as in Figure 2 for simple comparison. We additionally show the profile as a both a function of mass coordinate and radial coordinate in the two columns.

Considering first the single star model, we see that initially the convective core ($N < 0$) extends to $\sim 0.75\,\mathrm{M}_\odot$ (or $\sim 0.3\,\mathrm{R}_\odot$) and the frequency profile changes smoothly across the star. As the star evolves, the core recedes, leaving behind a chemical gradient; a peak then emerges in the Brunt–Väisälä frequency profile that extends between the core and the unmixed outer regions of the star. This peak is directly due to the chemical composition gradient imprinted on the star by the receding core during the main sequence. As the star evolves, the peak

extends in concert with the recession of the core, in line with the composition gradient.

For the accretor model, we see similar evolution in panels a and b (before mass transfer occurs). Immediately following mass transfer (in panel c), the convective core size aligns with the single star model and several sharp features emerge outside of the core, arising due to the kink in the composition gradient visible in panel c of Figure 2. As the star evolves, mixing smooths these features to some extent, but importantly the star retains a double-peaked Brunt–Väisälä frequency profile for the rest of its main sequence evolution.

The Brunt–Väisälä frequency profile of the accretor is inaccessible through single star evolution, which would always result in a smooth, unimodal peak due to the monotonic change in central hydrogen content.

3.2. *Period spacing patterns*

All differences between the mass-gainer and equivalent single star that we have noted so far are within the internal structure, and so are not directly observable. Therefore we now consider the impact of these internal structure changes on the observable period spacing pattern.

The period spacing pattern is defined as the difference in period between modes of the same spherical degree, ℓ, and neighbouring radial order, n. Under the assumption of spherical symmetry and high radial order, this difference is constant and follows the asymptotic g-mode period spacing given by Tassoul (1980):

$$\Delta P_g = \frac{\pi^2}{\sqrt{\ell(\ell+1)}} \left[\int_{r_0}^{r_1} \frac{N}{r}\,\mathrm{d}r \right]^{-1}, \qquad (2)$$

where ℓ is the spherical degree, N is the Brunt–Väisälä frequency (see Eq. 1) and r_0 and r_1 are the boundaries of the oscillation cavity, which in our model correspond to the convective core boundary and the outer edge of the star respectively.

Deviations from the asymptotic period spacing occur due to abrupt shifts in the Brunt–Väisälä frequency profile, which trap particular modes in certain regions of the star, altering their periods relative to the regular pattern (e.g. Miglio et al. 2008). The sensitivity of these deviations to the Brunt–Väisälä frequency thus makes the period spacing pattern a useful observable for probing the internal structure of a star.

We use the GYRE stellar oscillations code (Townsend & Teitler 2013; Townsend et al. 2018; Goldstein & Townsend 2020; Sun et al. 2023) to calculate the periods of the $\ell = 1, m = 0$ g-modes for both our accreting star and equivalent single star models. We scan periods from 0.1 to 4 days and solve the full 6th order dimension-

---

[3]The Brunt–Väisälä frequency was originally derived for us in meteorology and only later applied to stellar evolution. We encourage the interested reader to read the original derivation in Brunt (1927)
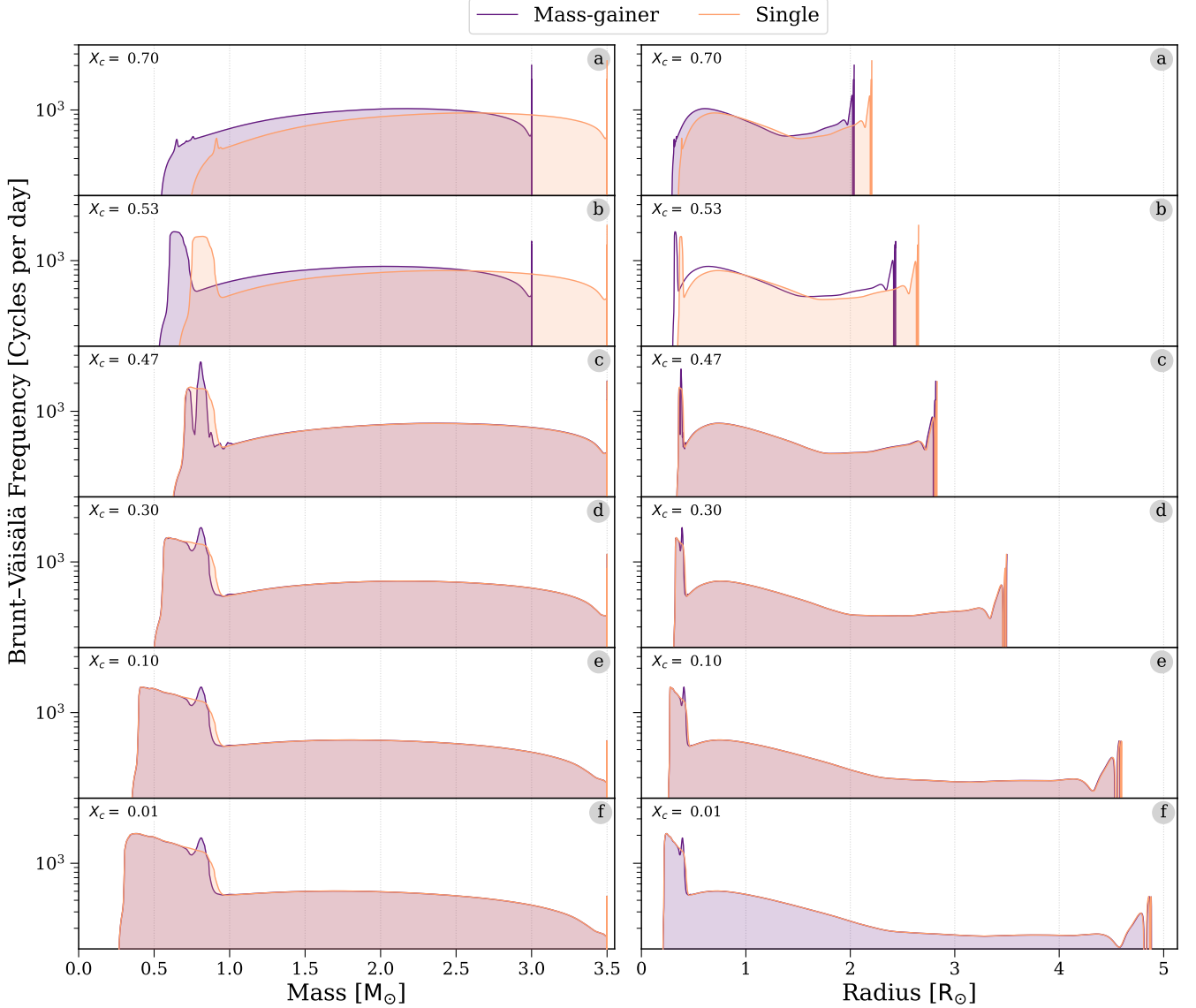
Figure 4. As Figure 2, but showing the Brunt–Väisälä frequency profile for the same evolutionary timesteps. **Left:** as a function of mass coordinate, **right:** as a function of radial coordinate.

less stellar oscillation equations using the Colloc scheme (Dziembowski 1971; Christensen-Dalsgaard 2008).

In Figure 5 we compare the period spacing pattern of a mass-gainer to that of an equivalent single star at different stages during their evolution. At the zero-age main sequence (in panel a), the period spacing pattern closely follows each star's asymptotic period spacing (denoted as dotted lines) due to the lack of any composition gradients. Early during the main sequence, immediately prior to mass transfer (in panel b), the pattern now displays some oscillation around the asymptotic value due to the chemical composition gradients that have developed outside of the core. Since this is currently pre-accretion, the stars have different masses and thus con-

vective core sizes, resulting in an offset between their asymptotic period spacings.

In subsequent panels (c–f) there are several differences in the period spacing pattern, despite the fact that the stars now have the same mass and convective core size. The two main differences can be expressed in terms of amplitude and phase of oscillations in the period spacing pattern. Frequently in the stars' later evolution, we note that the amplitude of deviations from the asymptotic spacing are larger for the mass-gainer. This is because the mass-gainer contains regions with steeper chemical composition gradients, which more strongly impact the Brunt–Väisälä frequency and thus the period of oscillations.
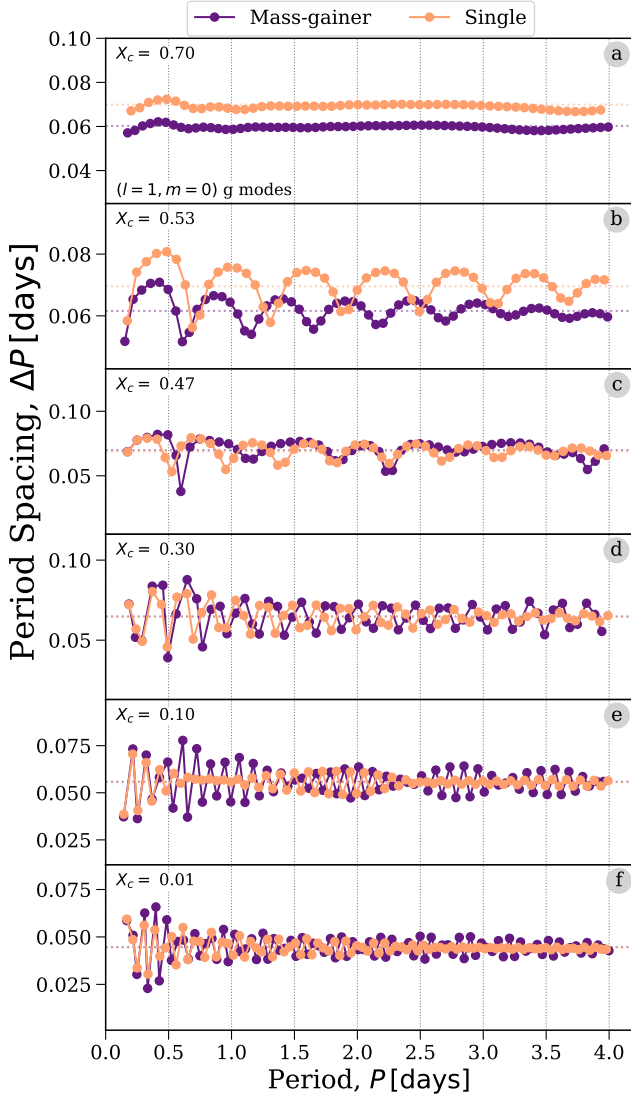
Figure 5. As Figure 2, but showing the period spacing patterns of the $\ell = 1, m = 0$ g-modes. Asymptotic period spacings for each model are shown as dotted lines. We emphasise that the y-axis limits vary by panel.

Help requested: It seems like the amplitude argument could be flawed, if this was true would we not only see amplitude differences in regions with phase differences?

In addition, we find that the period spacing pattern shifts phase in certain regions for the mass gainer. This is most apparent in panel e, in which the patterns are out of phase for periods between ∼1.5–3.2 days and in-phase otherwise. These period-dependent shifts arise due to difference between the Brunt–Väisälä frequency profiles occurring in the region of changing chemical composition. Modes that are sensitive to this region are shifted and so move out of phase, whilst other modes are in-

sensitive to the differences from a single star and thus oscillate with the same periods.

4. DISCUSSION

We have demonstrated that, compared to an equivalent single star, a mass-gainer shows significant differences in its period spacing pattern as a result of accretion altering its chemical composition gradient. In this Section we examine the implications of this result, considering both the impact on current inference modelling, as well as the potential for constraining mass transfer physics.

4.1. *Implications for inferring stellar properties*

Current work considers only single star evolution when inferring stellar properties from period spacing patterns. We have shown that these patterns are significantly changed as a result of mass transfer. Therefore, given that around 20% SPB stars are expected to be in interacted binaries, current methodology may result in incorrect inferences.

We test how incorrect these inferences may be by fitting the period spacing pattern of our mass-gainer model assuming single star evolution. We use `GYRE` to compute the periods of $\ell = 1, m = 0$ g-modes for our grid of single star models between 3 and $6 \, M_\odot$ across the entire main sequence. We then perform a reduced χ^2 fit for a given mass-gainer period spacing pattern with every single star model, at every timestep.

We match the periods of models independent of radial order, given that the exact radial order of an observed pulsation is not known a priori. In order to determine this matching we identify the offset, ϵ, between the mass-gainer and single star radial orders that would result in the best fit for a chain of periods of consecutive radial order[4]. These chains are motivated by the fact that one would expect that, for a well fitting model, adjacent mass-gainer periods would match to adjacent single star periods.

We calculate the χ^2 per degree of freedom for each model as

$$\chi^2 = \frac{\sum_i^N (P_{\mathrm{mg},i} - P_{\mathrm{s},(i+\epsilon)})^2}{N - 1}, \qquad (3)$$

where P_{mg} and P_{s} are the g-mode periods of the mass-gainer and single star models respectively, N is the minimum of the number of periods in each model and ϵ is

---

[4]We explored other techniques for determining this matching, such as using the longest chain of consecutive radial, and instead matching a single mode and using the next 20 modes. In each case we found very similar results.
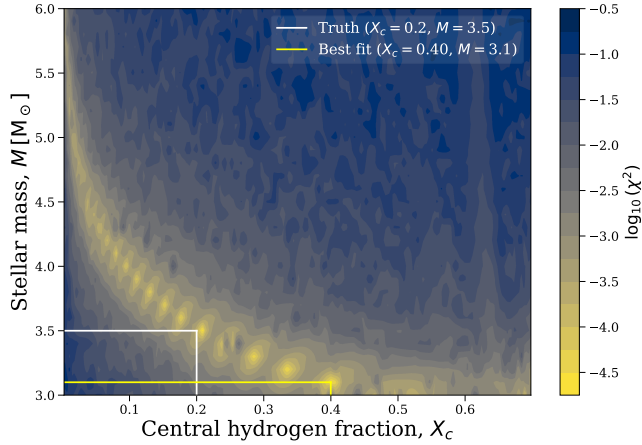
Figure 6. Stellar properties can be inferred incorrectly when assuming single star evolution. χ^2 values for fitting our mass-gainer model at X_c with our entire grid of single star models. The true values and best fit are highlighted with lines.

an offset in radial order between the models described above.

In Figure 6, we show an example of this χ^2 fitting. In this plot the mass-gainer model has a mass of $3.5\,\mathrm{M_\odot}$ and central hydrogen content of $X_c = 0.2$. However, the best fitting model when assuming single star evolution underestimates the mass at $3.1\,\mathrm{M_\odot}$ and significantly overestimates the central hydrogen content at $X_c = 0.4$, twice the true value. This best-fitting value is found along the degeneracy between mass and hydrogen content.

We repeated this fitting procedure throughout the evolution of the mass-gainer model and summarise the results in Table 1. Shortly after mass transfer ends (at $X_c = 0.47$), the best fit overestimates X_c but accurately determines the stellar mass. As the star settles onto the main sequence, the best-fit improves, with mass and X_c values very close to the true values. However, in the later stages of the star's main sequence evolution ($X_c \leq 0.2$), the best-fit diverges from the true value again, significantly overestimating X_c by at least a factor of 2 and consistently underestimating the stellar mass.

We therefore show that, though there are regimes within the main sequence in which using single star models may suffice for fitting mass-gainers, for a large fraction of the main sequence this will result in significant inaccuracies. The exact regimes in which these inaccuracies occur are likely mass and model dependent. Yet, given that the central hydrogen content of a star, as well how recently it may have undergone mass transfer, is generally unknown a priori, this implies one should be cautious when fitting a potential mass-gainer using single star models.

Mass-gainer	Best fit (Single star model)	
X_c	X_c	$M\,[\mathrm{M_\odot}]$
0.47	0.642	3.5
0.4	0.417	3.5
0.3	0.309	3.5
0.2	0.400	3.1
0.1	0.256	3.0
0.01	0.021	3.2

Table 1. Comparison of best-fit single star models to mass-gainer model at different evolutionary stages. Columns show central hydrogen content, X_c, and stellar mass, M. In each case the mass-gainer model has a mass of $3.5\,\mathrm{M_\odot}$.

4.2. *Constraining mass transfer*

- With independent measurements of parameters like age/composition you should be able to tell if period spacing pattern is off

- This can tell you about mass transfer

TODO: Write mass transfer constraint discussion

4.3. *Caveats*

Rotation—Given this analysis acts as a proof of principle, we have limited the scope of our investigations by neglecting rotation in each model. Yet, in reality, we expect that SPB stars will rotate, and this will impact several aspects of our results. In particular, rotation may enhance mixing in the vicinity of the core and alter the chemical composition gradient, which is the key difference between the mass-gainer and single star models.

Diffusive mixing—We enforce a minimum diffusive mixing both as an attempt to counter the lack of rotational mixing and eliminate any numerical artifacts. Given diffusive mixing directly smooths the chemical composition gradient, the choice of the minimum value has also an impact on our results for the Brunt–Väisälä frequency and period spacing pattern. However, as we demonstrate in Appendix A, differences between the mass-gainer and single star models are still present for a wide-range of choices for this parameter.

Mass-gainer model—The mass-gainer model that we use is formed from a binary in which we artificially ended mass transfer once $0.5\,\mathrm{M_\odot}$ of material was accreted. Although this choice is well motivated, since an accretor with rotation would quickly reach critical rotation and prevent further accretion, the choice may impact our results. Additionally, we only consider a single mass-gainer model for this proof of principle analysis and, though we expect the differences we find will be preva-

lent across a range of masses and periods, further work is necessary to confirm this.

4.4. *Future work*

- Examine this for a grid of binary models

- Include rotation

- Apply Miglio et al. (2008) framework to the distributions that we expect to see from mass transfer

TODO: Write future work subsection

5. SUMMARY & CONCLUSIONS

TODO: Write conclusions

Software: MESA: The MESA EOS is a blend of the OPAL (Rogers & Nayfonov 2002), SCVH (Saumon et al. 1995), FreeEOS (Irwin 2004), HELM (Timmes & Swesty 2000), PC (Potekhin & Chabrier 2010), and Skye (Jermyn et al. 2021) EOSes. Radiative opacities are primarily from OPAL (Iglesias & Rogers 1993, 1996), with low-temperature data from Ferguson et al. (2005) and the high-temperature, Compton-scattering dominated regime by Poutanen (2017). Electron conduction opacities are from Cassisi et al. (2007) and Blouin et al. (2020). Nuclear reaction rates are from JINA REACLIB (Cyburt et al. 2010), NACRE (Angulo et al. 1999) and additional tabulated weak reaction rates Fuller et al. (1985); Oda et al. (1994); Langanke & Martínez-Pinedo (2000). Screening is included via the prescription of Chugunov et al. (2007). Thermal neutrino loss rates are from Itoh et al. (1996). Roche lobe radii in binary systems are computed using the fit of Eggleton (1983). Mass transfer rates in Roche lobe overflowing binary systems are determined following the prescription of Ritter (1988).
GYRE (Townsend & Teitler 2013; Townsend et al. 2018), Astropy (Astropy Collaboration et al. 2013, 2018, 2022), Python (Van Rossum & Drake 2009), numpy (Harris et al. 2020), pandas (pandas development team 2022; Wes McKinney 2010), matplotlib (Hunter 2007), scipy (Virtanen et al. 2020)

REFERENCES

Aerts, C., Christensen-Dalsgaard, J., & Kurtz, D. W. 2010, Asteroseismology (Springerslowly pulsating B stars), doi: 10.1007/978-1-4020-5803-5

Aerts, C., Mathis, S., & Rogers, T. M. 2019, ARA&A, 57, 35, doi: 10.1146/annurev-astro-091918-104359

Almeida, L. A., Sana, H., Taylor, W., et al. 2017, A&A, 598, A84, doi: 10.1051/0004-6361/201629844

Angulo, C., Arnould, M., Rayet, M., et al. 1999, NuPhA, 656, 3, doi: 10.1016/S0375-9474(99)00030-5

Astropy Collaboration, Robitaille, T. P., Tollerud, E. J., et al. 2013, A&A, 558, A33, doi: 10.1051/0004-6361/201322068

Astropy Collaboration, Price-Whelan, A. M., Sipőcz, B. M., et al. 2018, AJ, 156, 123, doi: 10.3847/1538-3881/aabc4f

Astropy Collaboration, Price-Whelan, A. M., Lim, P. L., et al. 2022, apj, 935, 167, doi: 10.3847/1538-4357/ac7c74

Blouin, S., Shaffer, N. R., Saumon, D., & Starrett, C. E. 2020, ApJ, 899, 46, doi: 10.3847/1538-4357/ab9e75

Broekgaarden, F. S., Berger, E., Stevenson, S., et al. 2022, MNRAS, 516, 5737, doi: 10.1093/mnras/stac1677

Brunt, D. 1927, Quarterly Journal of the Royal Meteorological Society, 53, 30, doi: 10.1002/qj.49705322103

Cassisi, S., Potekhin, A. Y., Pietrinferni, A., Catelan, M., & Salaris, M. 2007, ApJ, 661, 1094, doi: 10.1086/516819

Christensen-Dalsgaard, J. 2008, Ap&SS, 316, 113, doi: 10.1007/s10509-007-9689-z

Chugunov, A. I., Dewitt, H. E., & Yakovlev, D. G. 2007, PhRvD, 76, 025028, doi: 10.1103/PhysRevD.76.025028

Claret, A., & Torres, G. 2017, ApJ, 849, 18, doi: 10.3847/1538-4357/aa8770

Cox, A. N., Morgan, S. M., Rogers, F. J., & Iglesias, C. A. 1992, ApJ, 393, 272, doi: 10.1086/171504

Crowe, R. A., & Matalas, R. 1982, A&A, 108, 55

Cyburt, R. H., Amthor, A. M., Ferguson, R., et al. 2010, ApJS, 189, 240, doi: 10.1088/0067-0049/189/1/240

Dziembowski, W. A. 1971, AcA, 21, 289

Eggleton, P. P. 1983, ApJ, 268, 368, doi: 10.1086/160960

Ferguson, J. W., Alexander, D. R., Allard, F., et al. 2005, ApJ, 623, 585, doi: 10.1086/428642

Fuller, G. M., Fowler, W. A., & Newman, M. J. 1985, ApJ, 293, 1, doi: 10.1086/163208

Goldstein, J., & Townsend, R. H. D. 2020, ApJ, 899, 116, doi: 10.3847/1538-4357/aba748

Harris, C. R., Millman, K. J., van der Walt, S. J., et al. 2020, Nature, 585, 357, doi: 10.1038/s41586-020-2649-2

Herwig, F. 2000, A&A, 360, 952, doi: 10.48550/arXiv.astro-ph/0007139

Hunter, J. D. 2007, Computing in Science & Engineering, 9, 90, doi: 10.1109/MCSE.2007.55

Iglesias, C. A., & Rogers, F. J. 1993, ApJ, 412, 752, doi: 10.1086/172958

—. 1996, ApJ, 464, 943, doi: 10.1086/177381

Irwin, A. W. 2004, The FreeEOS Code for Calculating the Equation of State for Stellar Interiors. http://freeeos.sourceforge.net/

Itoh, N., Hayashi, H., Nishikawa, A., & Kohyama, Y. 1996, ApJS, 102, 411, doi: 10.1086/192264

Jermyn, A. S., Schwab, J., Bauer, E., Timmes, F. X., & Potekhin, A. Y. 2021, ApJ, 913, 72, doi: 10.3847/1538-4357/abf48e

Jermyn, A. S., Bauer, E. B., Schwab, J., et al. 2023, ApJS, 265, 15, doi: 10.3847/1538-4365/acae8d

Johnston, C. 2021, A&A, 655, A29, doi: 10.1051/0004-6361/202141080

Kippenhahn, R., Ruschenplatt, G., & Thomas, H. C. 1980, A&A, 91, 175

Kolb, U., & Ritter, H. 1990, A&A, 236, 385

Kurtz, D. W. 2022, ARA&A, 60, 31, doi: 10.1146/annurev-astro-052920-094232

Langanke, K., & Martínez-Pinedo, G. 2000, Nuclear Physics A, 673, 481, doi: 10.1016/S0375-9474(00)00131-7

Langer, N., Fricke, K. J., & Sugimoto, D. 1983, A&A, 126, 207

Ledoux, P. 1947, ApJ, 105, 305, doi: 10.1086/144905

Mason, B. D., Hartkopf, W. I., Gies, D. R., Henry, T. J., & Helsel, J. W. 2009, AJ, 137, 3358, doi: 10.1088/0004-6256/137/2/3358

Michielsen, M., Aerts, C., & Bowman, D. M. 2021, A&A, 650, A175, doi: 10.1051/0004-6361/202039926

Miglio, A., Montalbán, J., Eggenberger, P., & Noels, A. 2008, Astronomische Nachrichten, 329, 529, doi: 10.1002/asna.200710991

Miszuda, A., Szewczuk, W., & Daszyńska-Daszkiewicz, J. 2021, MNRAS, 505, 3206, doi: 10.1093/mnras/stab1597

Mitalas, R. 1972, ApJ, 177, 693, doi: 10.1086/151748

Moe, M., & Di Stefano, R. 2017, ApJS, 230, 15, doi: 10.3847/1538-4365/aa6fb6

Neo, S., Miyaji, S., Nomoto, K., & Sugimoto, D. 1977, PASJ, 29, 249

Oda, T., Hino, M., Muto, K., Takahara, M., & Sato, K. 1994, Atomic Data and Nuclear Data Tables, 56, 231, doi: 10.1006/adnd.1994.1007

Packet, W. 1981, A&A, 102, 17

Pamyatnykh, A. A. 1999, AcA, 49, 119

pandas development team, T. 2022, pandas-dev/pandas: Pandas 1.4.2, v1.4.2, Zenodo, doi: 10.5281/zenodo.6408044

Paxton, B. 2023, Modules for Experiments in Stellar Astrophysics (MESA), r23.05.1, Zenodo, doi: 10.5281/zenodo.7983526

Paxton, B., Bildsten, L., Dotter, A., et al. 2011, ApJS, 192, 3, doi: 10.1088/0067-0049/192/1/3

Paxton, B., Cantiello, M., Arras, P., et al. 2013, ApJS, 208, 4, doi: 10.1088/0067-0049/208/1/4

Paxton, B., Marchant, P., Schwab, J., et al. 2015, ApJS, 220, 15, doi: 10.1088/0067-0049/220/1/15

Paxton, B., Schwab, J., Bauer, E. B., et al. 2018, ApJS, 234, 34, doi: 10.3847/1538-4365/aaa5a8

Paxton, B., Smolec, R., Schwab, J., et al. 2019, ApJS, 243, 10, doi: 10.3847/1538-4365/ab2241

Pedersen, M. G. 2022, ApJ, 930, 94, doi: 10.3847/1538-4357/ac5b05

Pedersen, M. G., Aerts, C., Pápics, P. I., & Rogers, T. M. 2018, A&A, 614, A128, doi: 10.1051/0004-6361/201732317

Potekhin, A. Y., & Chabrier, G. 2010, Contributions to Plasma Physics, 50, 82, doi: 10.1002/ctpp.201010017

Poutanen, J. 2017, ApJ, 835, 119, doi: 10.3847/1538-4357/835/2/119

Renzo, M., & Götberg, Y. 2021, ApJ, 923, 277, doi: 10.3847/1538-4357/ac29c5

Ritter, H. 1988, A&A, 202, 93

Rogers, F. J., & Nayfonov, A. 2002, ApJ, 576, 1064, doi: 10.1086/341894

Sana, H., de Mink, S. E., de Koter, A., et al. 2012, Science, 337, 444, doi: 10.1126/science.1223344

Saumon, D., Chabrier, G., & van Horn, H. M. 1995, ApJS, 99, 713, doi: 10.1086/192204

Silva Aguirre, V., Ballot, J., Serenelli, A. M., & Weiss, A. 2011, A&A, 529, A63, doi: 10.1051/0004-6361/201015847

Sun, M., Townsend, R. H. D., & Guo, Z. 2023, ApJ, 945, 43, doi: 10.3847/1538-4357/acb33a

Tassoul, M. 1980, ApJS, 43, 469, doi: 10.1086/190678

Timmes, F. X., & Swesty, F. D. 2000, ApJS, 126, 501, doi: 10.1086/313304

Townsend, R. H. D., Goldstein, J., & Zweibel, E. G. 2018, MNRAS, 475, 879, doi: 10.1093/mnras/stx3142

Townsend, R. H. D., & Teitler, S. A. 2013, MNRAS, 435, 3406, doi: 10.1093/mnras/stt1533

Van Rossum, G., & Drake, F. L. 2009, Python 3 Reference Manual (Scotts Valley, CA: CreateSpace)

Virtanen, P., Gommers, R., Oliphant, T. E., et al. 2020, Nature Methods, 17, 261, doi: 10.1038/s41592-019-0686-2

Väisälä, V. 1925, Soc. Sci. Fennica, Commentationes Phys.-Math. II, 19, 38. https://cir.nii.ac.jp/crid/1571417125137427072

Waelkens, C. 1991, A&A, 246, 453

Waelkens, C., & Rufener, F. 1985, A&A, 152, 6

Wes McKinney. 2010, in Proceedings of the 9th Python in Science Conference, ed. Stéfan van der Walt & Jarrod Millman, 56 – 61, doi: 10.25080/Majora-92bf1922-00a

APPENDIX

A. IMPORTANCE OF CHOICE OF MINIMUM DIFFUSIVE MIXING

In our `MESA` models we set a minimum diffusive mixing coefficient, D_{min}, in order to account for mixing processes not included in our model and to mix over unphysical numerical composition gradients. For our models analysed in this paper we set $D_{min} = 20\,\mathrm{cm^2\,s^{-1}}$, in this Appendix we explore the impact that this choice has on our results.

We repeated our binary `MESA` simulations for four additional choices of D_{min}, ranging from $1 - 100\,\mathrm{cm^2\,s^{-1}}$. In Figure A1 we compare the Brunt–Väisälä frequency profiles of these models at a central hydrogen abundance of $X_c = 0.1$, where the lower panel zooms in on the highlighted region in the upper panel. There are significant differences in the profiles between the different models. As one may expect, lower mixing coefficients lead to steeper composition gradients and therefore sharper features in the Brunt–Väisälä frequency and stronger signals in the period spacing pattern.

However, an overly low choice of D_{min} leads to numerical glitches in the composition gradient and the Brunt–Väisälä frequency profile. We highlight this in Figure A1, where glitches are clearly visible in both the $D_{min} = 1\,\mathrm{cm^2\,s^{-1}}$ and $D_{min} = 10\,\mathrm{cm^2\,s^{-1}}$ models.

We explored a more dense grid of D_{min} models and found that $D_{min} = 20\,\mathrm{cm^2\,s^{-1}}$ was the smallest level of mixing that still removed numerical glitches, which in-
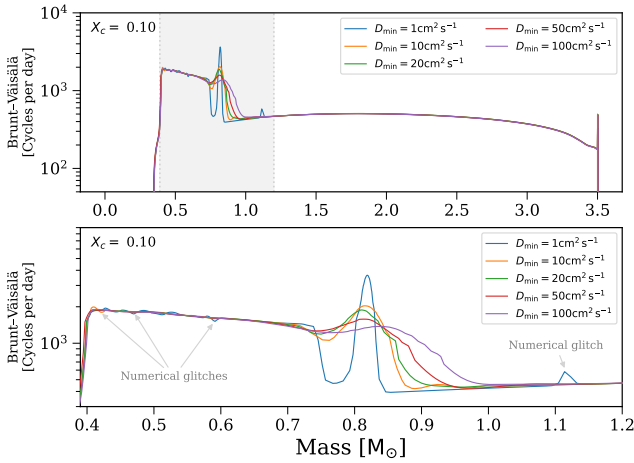
Figure A1. Comparison of the impact of changing the `MESA` minimum diffusive mixing parameter, D_{min}, on the Brunt–Väisälä frequency profile. Bottom panel zooms in on the highlighted range in the top panel. Annotations highlight numerical glitches in low D_{min} models.

formed our selection of this model as the default choice in this paper. This level of mixing is not unexpected, since mass transfer will likely induce rotation in the accretor (Packet 1981) and this leads to rotational mixing.
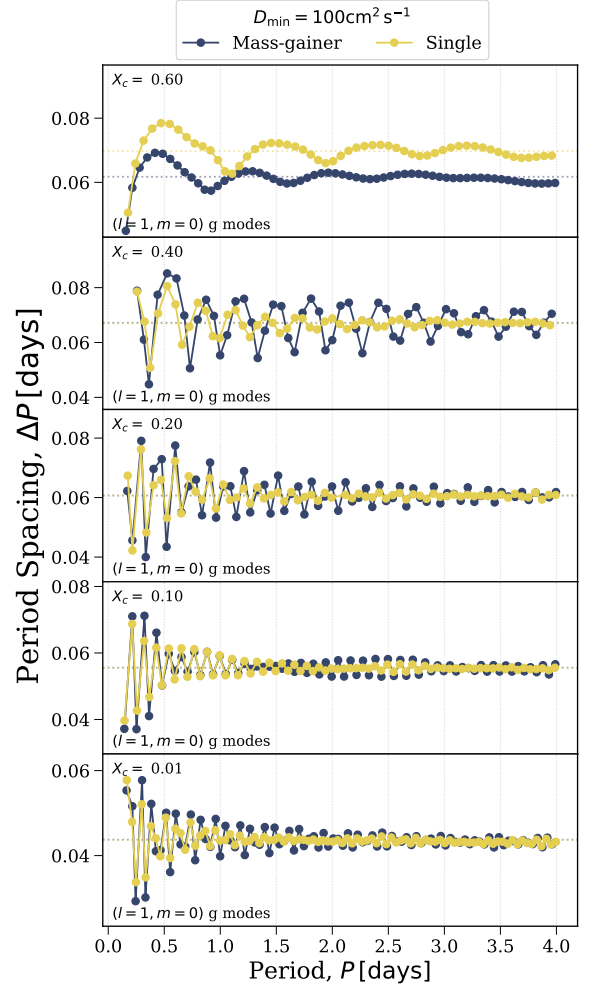
Figure A2. As Figure 5, but with the minimum diffusive mixing coefficient set to $D_{min} = 20\,\mathrm{cm^2\,s^{-1}}$.

We stress that the qualitative differences between the mass-gainer and single star in the period spacing patterns remain the same for all choices of D_{min} that we explored. To highlight this point we show the period spacing pattern for the model with $D_{min} = 100\,\mathrm{cm^2\,s^{-1}}$ in Figure A2. Despite slight differences to the exact shape of the pattern, we still find the same features of (i) stronger ΔP for mass-gainers and (ii) regions in which the period spacing is in-phase and regions in which it is out of phase between the mass-gainer and single star.

B. `MESA` RESOLUTION TESTS

`delta_mesh_coeff` time

Tom: Check results hold with higher res